J Pathol Inform

Editor-in-Chief:
Anil V. Parwani , Pittsburgh, PA, USA
Liron Pantanowitz, Pittsburgh, PA, USA

OPEN ACCESS
HTML format

For entire Editorial Board visit : www.jpathinformatics.org/editorialboard.asp

Technical Note

Oxygen supply maps for hypoxic microenvironment visualization in prostate cancer

Niels J. Rupp[1], Peter J. Schüffler[2], Qing Zhong[1], Florian Falkner[3], Markus Rechsteiner[1], Jan H. Rüschoff[1], Christian Fankhauser[1], Matthias Drach[1], Remo Largo[4], Mathias Tremp[5], Cedric Poyet[4], Tullio Sulser[4], Glen Kristiansen[6], Holger Moch[1], Joachim Buhmann[2], Michael Müntener[7], Peter J. Wild[1]

[1]Institute of Surgical Pathology, University Hospital Zurich, Schmelzbergstrasse 12, 8091 Zurich, [2]Department of Computer Science, ETH Zurich, Universitaetstr 6, 8092 Zurich, [3]Institute of Pathology, Cantonal Hospital Winterthur, Brauerstrasse 15, 8401 Winterthur, [4]Department of Urology, University Hospital Zurich, Rämistrasse 100, 8091 Zurich, [5]Department of Plastic, Reconstructive and Aesthetic Surgery, University Hospital Basel, Spitalstrasse 21, 4031 Basel, [7]Department of Urology, City Hospital Triemli, Birmensdorferstrasse 497, 8063 Zurich, Switzerland, [6]Institute of Pathology, University Hospital Bonn, Sigmund-Freud-Strasse 25, 53127 Bonn, Germany

E-mail: *Dr. Peter J. Wild - peter.wild@usz.ch
*Corresponding author

Senior authorship is shared between Michael Müntener and Peter J. Wild.
The first authorship is shared between Niels Rupp and Peter Schüffler.

Received: 18 August 2015 Accepted: 26 October 2015 Published: 29 January 2016

Abstract

Background: Intratumoral hypoxia plays an important role with regard to tumor biology and susceptibility to radio- and chemotherapy. For further investigation of hypoxia-related changes, areas of certain hypoxia must be reliably detected within cancer tissues. Pimonidazole, a 2-nitroimindazole, accumulates in hypoxic tissue and can be easily visualized using immunohistochemistry. **Materials and Methods:** To improve detection of highly hypoxic versus normoxic areas in prostate cancer, immunoreactivity of pimonidazole and a combination of known hypoxia-related proteins was used to create computational oxygen supply maps of prostate cancer. Pimonidazole was intravenously administered before radical prostatectomy in *n* = 15 patients, using the da Vinci robot-assisted surgical system. Prostatectomy specimens were immediately transferred into buffered formaldehyde, fixed overnight, and completely embedded in paraffin. Pimonidazole accumulation and hypoxia-related protein expression were visualized by immunohistochemistry. Oxygen supply maps were created using the normalized information from pimonidazole and hypoxia-related proteins. **Results:** Based on pimonidazole staining and other hypoxia-related proteins (osteopontin, hypoxia-inducible factor 1-alpha, and glucose transporter member 1) oxygen supply maps in prostate cancer were created. Overall, oxygen supply maps consisting of information from all hypoxia-related proteins showed high correlation and mutual information to the golden standard of pimonidazole. Here, we describe an improved computer-based ex vivo model for an accurate detection of oxygen supply in human prostate cancer tissue. **Conclusions:** This platform can be used for precise colocalization of novel candidate hypoxia-related proteins in a representative number of prostate cancer cases, and improve issues of single marker correlations. Furthermore, this study provides a source for further in situ tests and biochemical investigations

Key words: Hypoxia, pimonidazole, prostate cancer

Access this article online

Website: www.jpathinformatics.org

DOI: 10.4103/2153-3539.175376

Quick Response Code:

This article may be cited as: Rupp NJ, Schuffler PJ, Zhong Q, Falkner F, Rechsteiner M, Ruschoff JH, *et al*. Oxygen supply maps for hypoxic microenvironment visualization in prostate cancer. J Pathol Inform 2016;7:3.
Available FREE in open access from: http://www.jpathinformatics.org/text.asp?2016/7/1/3/175376

INTRODUCTION

Tumor hypoxia has been shown to drive malignant progression,[1] induce genetic instability,[2] and gene amplification,[3] as well as impair DNA repair mechanisms.[4] In particular, in prostate cancer, hypoxia was identified *in vivo*[5] and showed a significant association with advanced tumor stage[6] and aggressive disease.[7] Other studies showed an increased resistance to androgen deprivation and radio- and chemotherapy[8-10] of tumors with large hypoxic regions. To create optical oxygen supply maps, we used a human *ex vivo* model, based on the compound pimonidazole.[11] Pimonidazole (hypoxyprobe™ -1; Chemicon International, Inc., Billerica, MA, USA), a 2-nitroimidazole, accumulates *in vivo* in hypoxic tissue ($pO_2 \leq 10$ mmHg at 37°C) and can be easily visualized in surgical specimens (*ex vivo*) by immunohistochemical analysis.[12] Pimonidazole is generally used in animal models, pimonidazole-based hypoxia labeling in human tissue samples is rarely performed because of ethical, pharmacological, and legal restrictions. To overcome these limitations, correlations between pimonidazole labeling and superimpositions with other known hypoxia-related proteins, including osteopontin (OPN),[13,14] hypoxia-inducible factor 1-alpha (HIF1A),[15,16] and glucose transporter member 1 (GLUT1),[17,18] were investigated. Here, we describe a new method to reliably detect hypoxic tumor regions that does not employ invasive techniques, to further investigate hypoxia and hypoxia-related markers in prostatectomy specimens.

PROCEDURE

To verify that pimonidazole serves as a robust marker for hypoxia in prostate cancer cells, we incubated LNCaP cells (American Type Culture Collection, Manassas, VA, USA) under normoxic and hypoxic conditions, with or without pimonidazole. In accordance with the findings of previous studies,[11,12] we confirmed pimonidazole as a direct marker for hypoxia. Immunocytochemical staining of pimonidazole revealed a clear positivity in LNCaP cells under hypoxic conditions while cells cultured under normoxic conditions were negative for pimonidazole [Figure 1a].

After *in vivo* administration of pimonidazole, following radical prostatectomy, a total of 15 prostatectomy specimens [for cohort information see Supplementary Table 1] were subjected to immunohistochemical staining for pimonidazole, OPN, GLUT1, and HIF1A [Figure 1b]. Pimonidazole, GLUT1, and OPN showed a medium to strong cytoplasmic overall staining intensity, particularly of cancer tissues. Qualitative analysis of pimonidazole staining showed partial spatial overlapping of all hypoxia markers. A study in advanced head and neck squamous cell carcinoma described the rationale for colocalization

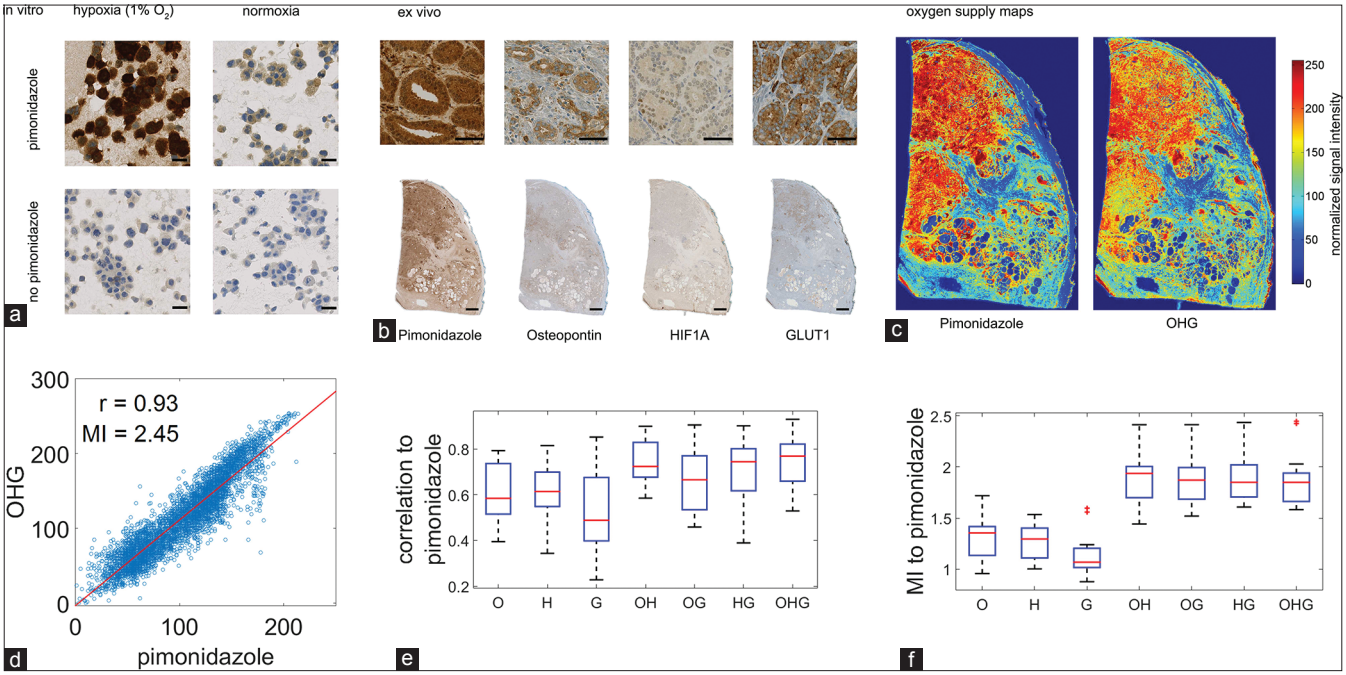

Figure 1: (a) *In vitro* validation of the anti-pimonidazole antibody by immunocytochemical staining using LNCaP prostate cancer cells. (b) Immunohistochemical staining for pimonidazole, osteopontin (O), hypoxia-inducible factor 1-alpha (H), and glucose transporter member 1 (G), scale bars 2 mm and 100 μm. (c) Generation of oxygen supply maps. (d) Dot-wise comparisons of both oxygen supply maps (OHG vs. P) in one representative case. (e and f) Box plots with Spearman correlation coefficients and mutual information comparing pimonidazole with osteopontin (O), hypoxia-inducible factor 1-alpha (H), glucose transporter member 1 (G), and combinatory overlays for 15 patients

of different hypoxia-related proteins with pimonidazole:[19] Individual hypoxia markers were higher expressed in pimonidazole-positive areas. However, the overall single correlation was poor. To this end, we targeted this issue by pooling all available information from hypoxia-related proteins to construct oxygen supply maps.

The staining images for the known hypoxia-related proteins OPN (O), GLUT1 (G), and HIF1A (H) of each case were automatically color corrected, aligned, superimposed, and normalized for the generation of a pseudo-colored oxygen supply map [Figure 1c, OHG]. First, the original images were white-balanced to remove the grayish background. Second, the tissue regions were automatically identified and rotated, translated, cropped, and rescaled for rough alignment of the tissues to the middle slice. The background was then deleted to remove background artifacts which could disturb the following alignment process. Third, for pixel-wise matching and to conform to morphological changes of the tissues in consecutive slices, we incorporated a nonlinear SIFT flow algorithm[20] (see online methods for detailed description of all steps). Furthermore, an analogous oxygen supply map based on pimonidazole staining was created [Figure 1c, pimonidazole]. These maps were then normalized by histogram equalization and compared for each case using a dot-wise correlation of both images, which yielded high Spearman correlation coefficients [Figure 1e and Supplementary Figure 1a-o] and mutual information (MI) [Figure 1f]. MI between two images X and Y has been calculated as $\mathrm{MI}(X,Y)=\sum_{x,y=1}^{256} p(x,y)*\log\left(\frac{p(x,y)}{p(x)p(y)}\right)$ where $P(x)$ is the probability of intensity x in the normalized histogram of X and $P(x,y)$ is the probability of x and y in the normalized joint histogram of X and Y. All image processing steps were implemented in MATLAB 2014a, automatically performed and visually approved. A most simple combinatorial information of O, H, and G overlay maps were generated as the mean of individual intensity maps (more sophisticated combinations have not been considered in this study). Pimonidazole compared with an overlay of all three hypoxia markers (OHG) was highly correlative [Spearman correlation coefficient, $r = 0.93$, MI = 2.45; Figure 1d]. Comparison of pimonidazole with single markers (O, H, G) and combinatory overlays (OH, OG, HG) also showed high correlation coefficients [Figure 1e]. Only two cases revealed lower correlation coefficients [Supplementary Table 2; B12-4671, B12-6064] because of crush artifacts. MI increases significantly in overlay images when combined with two or three markers [Figure 1f]. As previously shown,[11] scant correlations with microvessel density and pimonidazole could be observed in representative overlays of pimonidazole with CD34 immunoreactivity ($n = 2$, data not shown).

CONCLUSION

Here, we introduce a computer-assisted approach to detect oxygen gradients in human prostate cancer tissues by colocalization of the expression of validated hypoxia-related markers compared to intravenously administered pimonidazole. The generated oxygen supply maps can be used to precisely colocalize potential hypoxia-related proteins in a quantitative and pictorial manner and will render compounds, such as pimonidazole, unnecessary in human patients.

Financial Support and Sponsorship
Nil.

Conflicts of Interest
There are no conflicts of interest.

REFERENCES

1. Bertout JA, Patel SA, Simon MC. The impact of O2 availability on human cancer. Nat Rev Cancer 2008;8:967-75.
2. Reynolds TY, Rockwell S, Glazer PM. Genetic instability induced by the tumor microenvironment. Cancer Res 1996;56:5754-7.
3. Young SD, Marshall RS, Hill RP. Hypoxia induces DNA overreplication and enhances metastatic potential of murine tumor cells. Proc Natl Acad Sci U S A 1988;85:9533-7.
4. Yuan J, Glazer PM. Mutagenesis induced by the tumor microenvironment. Mutat Res 1998;400:439-46.
5. Movsas B, Chapman JD, Horwitz EM, Pinover WH, Greenberg RE, Hanlon AL, *et al.* Hypoxic regions exist in human prostate carcinoma. Urology 1999;53:11-8.
6. Movsas B, Chapman JD, Greenberg RE, Hanlon AL, Horwitz EM, Pinover WH, *et al.* Increasing levels of hypoxia in prostate carcinoma correlate significantly with increasing clinical stage and patient age: An Eppendorf pO (2) study. Cancer 2000;89:2018-24.
7. Ragnum HB, Vlatkovic L, Lie AK, Axcrona K, Julin CH, Frikstad KM, *et al.* The tumour hypoxia marker pimonidazole reflects a transcriptional programme associated with aggressive prostate cancer. Br J Cancer 2015;112:382-90.
8. Tinganelli W, Ma NY, Von Neubeck C, Maier A, Schicker C, Kraft-Weyrather W, *et al.* Influence of acute hypoxia and radiation quality on cell survival. J Radiat Res 2013;54 Suppl 1:i23-30.
9. Marignol L, Coffey M, Lawler M, Hollywood D. Hypoxia in prostate cancer: A powerful shield against tumour destruction? Cancer Treat Rev 2008;34:313-27.
10. Rudolfsson SH, Bergh A. Hypoxia drives prostate tumour progression and impairs the effectiveness of therapy, but can also promote cell death and serve as a therapeutic target. Expert Opin Ther Targets 2009;13:219-25.
11. Carnell DM, Smith RE, Daley FM, Saunders MI, Bentzen SM, Hoskin PJ. An immunohistochemical assessment of hypoxia in prostate carcinoma using pimonidazole: Implications for radioresistance. Int J Radiat Oncol Biol Phys 2006;65:91-9.
12. Arteel GE, Thurman RG, Raleigh JA. Reductive metabolism of the hypoxia marker pimonidazole is regulated by oxygen tension independent of the pyridine nucleotide redox state. Eur J Biochem 1998;253:743-50.
13. Sodhi CP, Phadke SA, Batlle D, Sahai A. Hypoxia and high glucose cause exaggerated mesangial cell growth and collagen synthesis: Role of osteopontin. Am J Physiol Renal Physiol 2001;280:F667-74.
14. Zhu Y, Denhardt DT, Cao H, Sutphin PD, Koong AC, Giaccia AJ, *et al.* Hypoxia upregulates osteopontin expression in NIH-3T3 cells via a Ras-activated enhancer. Oncogene 2005;24:6555-63.
15. Zhong H, Agani F, Baccala AA, Laughner E, Rioseco-Camacho N, Isaacs WB, *et al.* Increased expression of hypoxia inducible factor-1alpha in rat and human prostate cancer. Cancer Res 1998;58:5280-4.
16. Wang GL, Semenza GL. General involvement of hypoxia-inducible factor

1 in transcriptional response to hypoxia. Proc Natl Acad Sci U S A 1993;90:4304-8.
17. Stewart GD, Gray K, Pennington CJ, Edwards DR, Riddick AC, Ross JA, *et al.* Analysis of hypoxia-associated gene expression in prostate cancer: Lysyl oxidase and glucose transporter-1 expression correlate with Gleason score. Oncol Rep 2008;20:1561-7.
18. Ebert BL, Firth JD, Ratcliffe PJ. Hypoxia and mitochondrial inhibitors regulate expression of glucose transporter-1 via distinct Cis-acting sequences. J Biol Chem 1995;270:29083-9.
19. Rademakers SE, Lok J, van der Kogel AJ, Bussink J, Kaanders JH. Metabolic markers in relation to hypoxia; staining patterns and colocalization of pimonidazole, HIF-1α, CAIX, LDH-5, GLUT-1, MCT1 and MCT4. BMC Cancer 2011;11:167.
20. Liu C, Yuen J, Torralba A. SIFT flow: Dense correspondence across scenes and its applications. IEEE Trans Pattern Anal Mach Intell 2011;33:978-94.

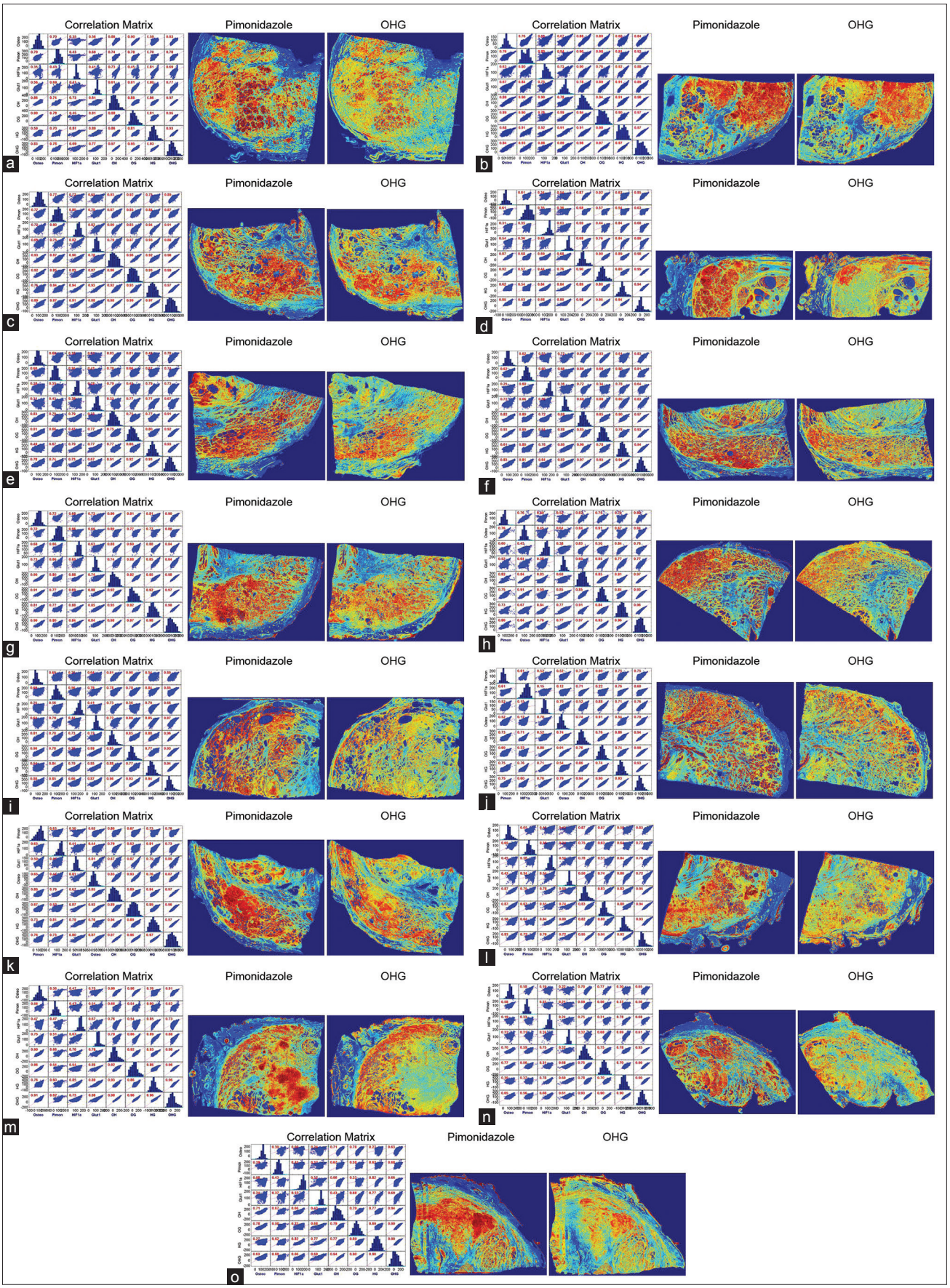

Supplementary Figure 1: (a-o) Spearman correlation matrices of O, H, G and combinations thereof. Oxygen supply maps based on pimonidazole staining and overlay images (OHG) for each of the 15 prostatectomy specimens are provided

Supplementary Table 1: Clinico-pathological data

No.	Specimen	Age	Gleason-score	pT-status	pN-status
1	B2010.56819	63	4+5=9	3b	1
2	B2011.1715	73	3+4=7	2c	n.a.
3	B2011.3301	63	3+3=6	2c	n.a.
4	B2011.11148	66	4+5=9	3b	0
5	B2011.12352	62	3+4=7	2c	0
6	B2011.16032	64	4+3=7	2c	0
7	B2011.31427	69	4+3 (5)=7	3a	0
8	B2011.32991	47	4+3=7	2c	n.a.
9	B2011.38027	65	4+3=7	2c	n.a.
10	B2011.41387	57	4+4=8	2c	0
11	B2011.46731	66	5+4=9	2c	0
12	B2011.56960	63	4+3=7	2c	0
13	B2012.4671	65	3+4=7	2c	0
14	B2012.6064	67	3+4=7	2c	0
15	B2012.7443	70	4+3=7	3a	0

n.a.: Not available.

Supplementary Table 2: Spearman correlation coefficients with pimonidazole

Specimen	O	H	G	OH	OG	HG	OHG
B2010.56819	0.7034	0.5282	0.6522	0.7357	0.7750	0.6710	0.7769
B2011.11148	0.5579	0.4876	0.2912	0.6285	0.4955	0.4917	0.5451
B2011.12352	0.6037	0.6056	0.4424	0.7132	0.6414	0.6721	0.7296
B2011.16032	0.5840	0.6674	0.6265	0.7804	0.6650	0.7934	0.7927
B2011.1715	0.7470	0.8144	0.8515	0.8985	0.9045	0.9006	0.9291
B2011.31427	0.7923	0.7216	0.6828	0.8324	0.7978	0.8030	0.8332
B2011.32991	0.7480	0.6899	0.5339	0.8345	0.7542	0.7721	0.8215
B2011.3301	0.7881	0.8137	0.7449	0.8719	0.8570	0.8335	0.8742
B2011.38027	0.5014	0.5950	0.7632	0.7233	0.7243	0.8094	0.8189
B2011.41387	0.3948	0.6300	0.4568	0.6953	0.5338	0.7522	0.7204
B2011.46731	0.6734	0.7012	0.4881	0.8169	0.6774	0.7438	0.7683
B2011.56960	0.5382	0.6138	0.3210	0.7009	0.5221	0.6098	0.6522
B2012.4671	0.5075	0.5436	0.3846	0.5848	0.4585	0.5354	0.5289
B2012.6064	0.5716	0.3435	0.2279	0.5995	0.5355	0.3890	0.5668
B2012.7443	0.4276	0.5621	0.4383	0.6698	0.5696	0.6380	0.6780

Bold face, highest spearman correlation with pimonidazole staining